12th International Conference on Structural Analysis of Historical Constructions
SAHC 2020
P. Roca, L. Pelà and C. Molins (Eds.)

STRUCTURAL PERFORMANCE EVALUATION OF COLUMN-*NUKI* CONNECTION IN TRADITIONAL JAPANESE WOODEN BUILDINGS

SATSUKI MURAI[1*] AND MITSUHIRO MIYAMOTO[2]

[1]Division of Safety Systems Construction, Graduate School of Engineering, Kagawa University
2217-20 Hayashi-cho, Takamatsu, Kagawa 761-0396, Japan
e-mail: s19g407@stu.kagawa-u.ac.jp (*corresponding author)

[2]Department of Engineering and Design, Faculty of Engineering and Design, Kagawa University
2217-20 Hayashi-cho, Takamatsu, Kagawa 761-0396, Japan
email: miyamoto@eng.kagawa-u.ac.jp; Web page: https://www.kagawa-u.ac.jp/kagawa-u_ead/

Keywords: Traditional Japanese wooden buildings, column-*nuki* connection, seismic performance evaluation

Abstract. *Traditional Japanese wooden buildings have been constructed using internal wooden frame structures. Plus-shaped column-nuki connections are important to evaluate the seismic performance of these buildings, and these connections include several joint types, one of which is the oblique scarf joint. However, only very few extant studies have examined column-nuki connections and oblique scarf joints. Consequently, no design equations exist for this combination. Therefore, it is possible that the structural performance of column-nuki connections might be inaccurately evaluated. Thus, this study aims to evaluate the structural performance evaluation of column-nuki connections in traditional Japanese wooden buildings. Full-scale tests were performed on specimens with either the continuous or oblique scarf joint nuki, and results obtained were compared based on parameters, such as the type of connection and number of dimensions. Subsequently, corresponding analytical results were calculated using an extant design equation, and the same were compared against experimental values to determine the validity of using the design equation for column-nuki connections in traditional Japanese wooden buildings. Results obtained in this study demonstrate the initial stiffness to be approximately identical for specimens with continuous or oblique scarf joint nuki. The yield and ultimate bending moment of oblique scarf joint nuki specimens were observed to be approximately 10–70% smaller compared to those corresponding to continuous nuki specimens. In addition, all oblique scarf joint nuki specimens demonstrated an initial cleavage failure followed by multiple failures. Results of these comparisons demonstrate that failure can be partially estimated using the extant design equation considered in this study.*

1 INTRODUCTION

Traditional wooden buildings in Japan, such as temples and shrines, demonstrate high deformability, and they can resist large lateral forces during earthquakes. Since ancient times, these traditional buildings have been constructed using column-*nuki* connections. The construction technique involves building a whole wall around the periphery with the inner structure comprising wooden frames. Column-*nuki* connections used in the construction of Japanese shrines and temples are larger compared to those used in residential houses. Consequently, some walls of ancient Japanese buildings can resist large lateral forces during earthquakes. Thus, column-*nuki* connections can be considered important elements during structural performance evaluation of traditional Japanese buildings. However, as shown in reference [1], very few experiments have been conducted on large column-*nuki* connections and of those, even fewer have been conducted on oblique scarf joint *nuki* connections, a popular connection type, in traditional wooden Japanese buildings. In seismic evaluations of traditional Japanese houses, the extant design equation has been considered only for continuous *nuki*. As shown in reference [2], oblique scarf joint *nuki* are evaluated as 0.5 of the design equation for continuous *nuki* in traditional Japanese houses. Therefore, there exists a possibility that structural-performance evaluations of column-*nuki* connections with oblique scarf joint *nuki* are inaccurate.

The study aims to evaluate the structural performance of column-*nuki* connections in traditional Japanese wooden buildings. To this end, full-scale tests were performed on plus-shaped column-*nuki* connections used in Japanese shrine and temple construction. Results of these tests were compared against those obtained using the relationship between the deformation angle and bending moment as well as failure properties of continuous and oblique scarf joint *nuki*. Details concerning these full-scale tests are described in section 2 of this manuscript, whereas section 3 discusses the validity of estimate equations used for evaluating the said plus-shaped column-*nuki* connection. The said estimate equations were evaluated for comparing analytical results against experimental values pertaining to both continuous and oblique scarf joint *nuki* connections.

2 FULL-SCALE TEST OF PLUS-SHAPED COLUMN–*NUKI* CONNECTION

In this study, full-scale tests of specimens with continuous or oblique scarf joint *nuki* were conducted to examine the seismic performance of plus-shaped column-*nuki* connections. The relationship between the bending moment and deformation angle as well as the failure property were investigated. The test parameters were chosen to examine the seismic performance of a plus-shaped column-*nuki* specimen, which had either continuous or oblique scarf joint *nuki*. Both of these have been used for traditional Japanese wooden buildings in the past.

2.1 Outline of full-scale tests

Tables 1 and 2 provide information about the specimens examined in the study. A total of sixteen specimens were tested; eight contained continuous *nuki*, and eight contained oblique scarf joint *nuki*. All specimens were plus shaped, and the lengths of both the *nuki* and the column were 1,400 mm. The test specimens were labeled as C for continuous *nuki* and J for oblique

scarf joint *nuki*. For the continuous *nuki* specimens, one condition was different for each specimen based on C1. Figure 1 (a) depicts a drawing of the continuous *nuki* joint, whereas Figure 1 (b) depicts that corresponding to a continuous *nuki* with cogged C4 joint. All specimens, except C5, have wedges. The oblique scarf joint *nuki* specimens come in two geometries, as shown in Figures 1 (c) and (d). The numbers right after J in the specimens' name correspond to those mentioned in the list of continuous *nuki*s.

The image of the loading device is shown in Figure 2. The specimen was fixed using a jig. In these tests, positive and negative sides are defined as the left and right sides, respectively, and the negative side contains the wedge. The specimen was subjected to cyclic lateral loads, and the apparent shear deformation angle of a *nuki* ℽ was gradually increased symmetrically from 1/200, 1/150, 1/100, 1/75, 1/50, 1/30, 1/20, 1/15, to 1/10 rad. One cycle of loading was applied. Finally, the specimen was subjected to a lateral load at an angle of 1/7 rad at one end. Figure 3 depicts the full-scale test setup.

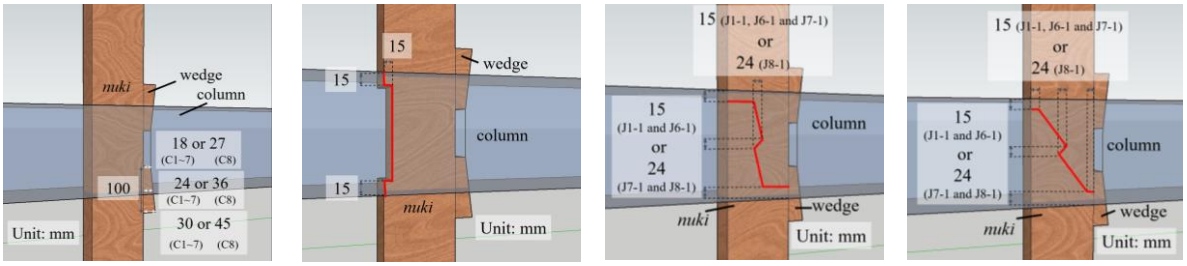

(a) Continuous *nuki* (b) Continuous *nuki* with cogged joint (c) Oblique scarf joint *nuki* α (d) Oblique scarf joint *nuki* β

Figure 1: Details concerning connection types used in traditional Japanese buildings

Table 1: Continuous *nuki* specimen specifications

Specimen	Type of connection	Dimensions			Shape of column	Type of wood
		Diameter of column (mm)	Width of *nuki* (mm)	Height of *nuki* (mm)		
C1	Continuous *nuki*	180	50	120	Square	Japanese cypress
C2	Continuous *nuki*	180	50	120	Circle	Japanese cypress
C3	Continuous *nuki*	180	50	120	Square	Japanese cedar
C4	Continuous *nuki* with cogged joint	180	50	120	Square	Japanese cypress
C5	Continuous *nuki* without wedge	180	50	120	Square	Japanese cypress
C6	Continuous *nuki*	180	90	120	Square	Japanese cypress
C7	Continuous *nuki*	240	90	120	Square	Japanese cypress
C8	Continuous *nuki*	240	90	180	Square	Japanese cypress

Table 2: Oblique scarf joint *nuki* specimen specifications

Specimen	Type of connection	Dimensions			Shape of column	Type of wood
		Diameter of column (mm)	Width of *nuki* (mm)	Height of *nuki* (mm)		
J1-1	Oblique scarf joint α *nuki*	180	50	120	Square	Japanese cypress
J1-2	Oblique scarf joint β *nuki*	180	50	120	Square	Japanese cypress
J6-1	Oblique scarf joint α *nuki*	180	90	120	Square	Japanese cypress
J6-2	Oblique scarf joint β *nuki*	180	90	120	Square	Japanese cypress
J7-1	Oblique scarf joint α *nuki*	240	90	120	Square	Japanese cypress
J7-2	Oblique scarf joint β *nuki*	240	90	120	Square	Japanese cypress
J8-1	Oblique scarf joint α *nuki*	240	90	180	Square	Japanese cypress
J8-2	Oblique scarf joint β *nuki*	240	90	180	Square	Japanese cypress

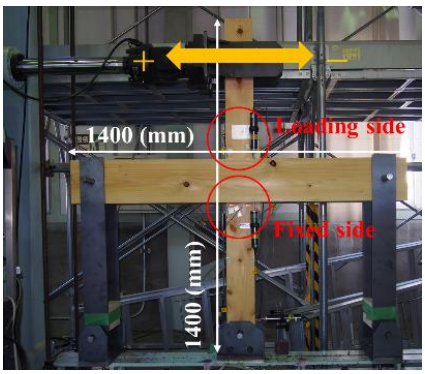

Figure 2: Loading device apparatus

Figure 3: Loading during full-scale tests

2.2 Result and discussion of full-scale tests

Figure 4 illustrates the relationship between the bending moment and deformation angle in the different continuous *nuki* specimens, as determined via full-scale tests performed in this study. The ultimate bending moment corresponds to a deformation angle of 1/10 rad, including a safety factor of 1.5, since the collapse limit of traditional wooden buildings is 1/15 rad.

Images of the failure of continuous *nuki* are shown in Figure 5. Specimens C1 to C7 exhibited cleavage of the wedge. However, the cleavage was not affected by the decrease in bending moment. In C1 and C2, the ultimate bending moments demonstrated approximately the same difference for different column shapes. The initial stiffness of C3 was approximately 70% less than that of C1, and the ultimate bending moment of C3 was approximately 60% smaller than of C1, even though the elastic modulus of C3 was approximately 10% percent than

of C1 in the material test. The ultimate bending moment of C4 was approximately 10% smaller than that of C1, because of the use of the cogged joint. The ultimate bending moment of C1 was approximately 80% larger than that of C5, because of the use of the wedge. Among continuous *nuki* specimens, the ultimate bending moment of C8 was the biggest and the ultimate bending moment increased from C1 to C6 to C7 to C8 because the dimensions of the specimens also increased. It is assumed that the bending moment increased because the dimensions of the specimen increased.

Figure 6 depicts the relationship between the bending moment and deformation angle pertaining to the plus-shaped column-*nuki* connection with a continuous *nuki* and the oblique scarf *nuki*. Results of full-scale tests are depicted in Figures 7. The continuous *nuki* specimen exhibited embedment failure at first; however, all specimens with the oblique scarf *nuki*, except for J8-2 first experienced cleavage failure from the *kama* joint and then bending failure, as shown in Figure 8(a). One *kama* joint was stuck in the other *kama* joint at J8-2, as shown in Figures 8(b). Only the specimen with the oblique scarf joint β *nuki* exhibited shear failure, as shown in Figure 8(c). The initial stiffness of the continuous and oblique scarf joint *nuki* specimens with the same dimensions was approximately the same. Both the yield bending moment and ultimate bending moment were approximately 10 to 70% smaller for the oblique scarf joint *nuki* than for the continuous one. In addition, the specimens with oblique scarf joint β had both a yield bending moment and ultimate bending moment that was 10% smaller than that of the specimens with oblique scarf joint αbecause oblique scarf joint βhas steeper angle than oblique scarf joint α. This suggests that the bending moment tends to be smaller if the *kama* joint connection has steep angle. For the specimens with the oblique scarf *nuki*, the deformation angle was smaller for the load on the positive side than for the load on the negative side until failure.

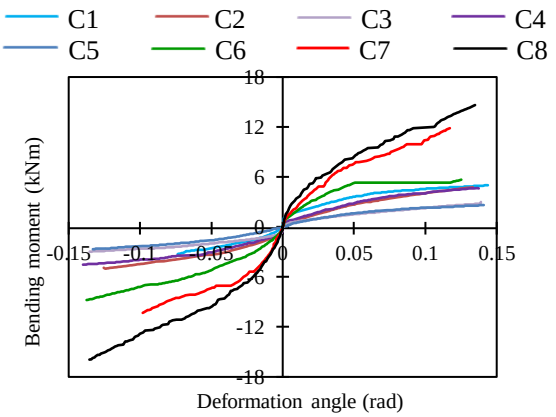

Figure 4: Bending moment vs. deformation angle in full-scale tests (continuous *nuki*)

(a) Cleavage failure of wedge

(b) Embedment failure of *nuki*

(c) Cleavage failure of column

(d) Failure property of *nuki*

Figure 5: Images of failure (continuous *nuki*)

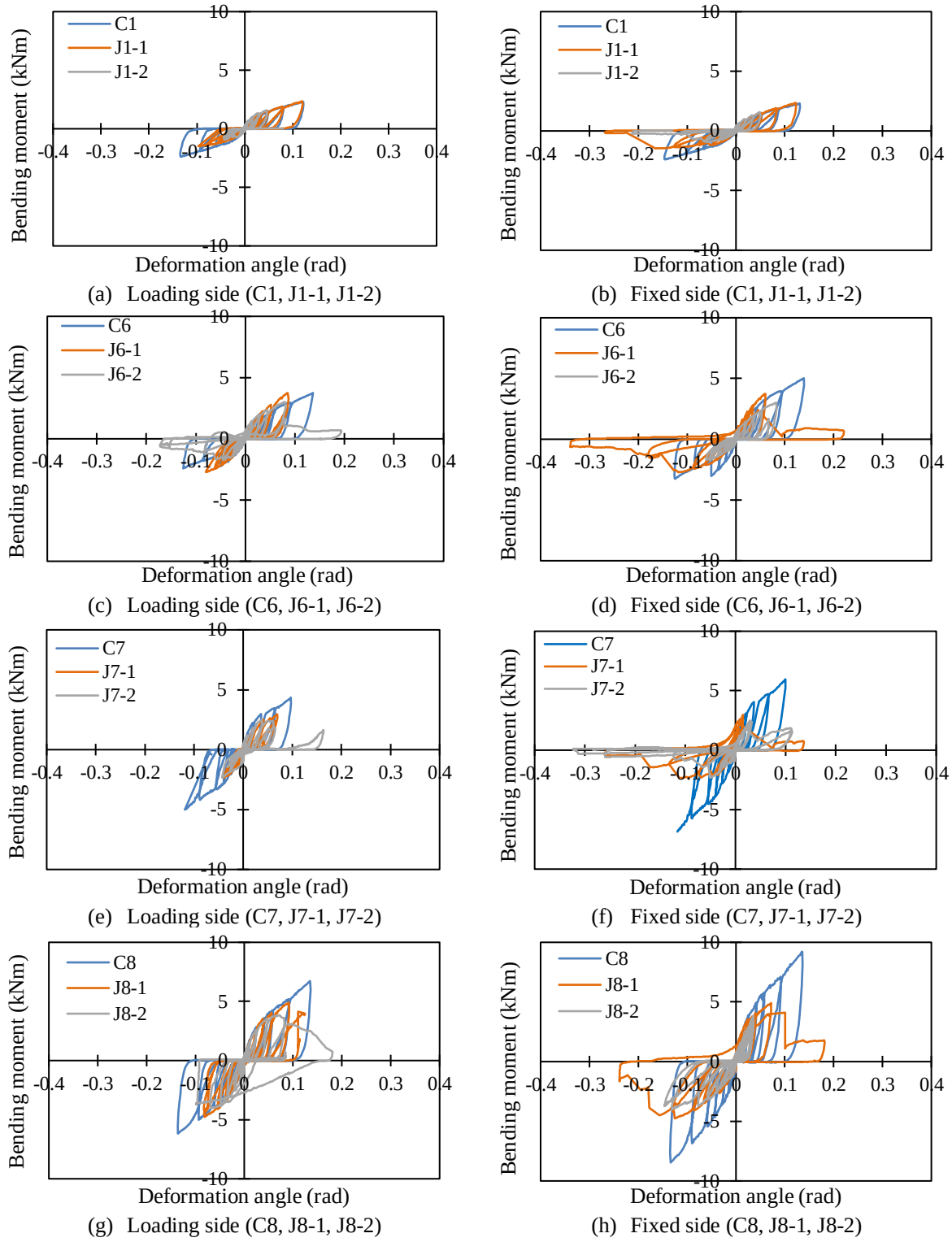

(a) Loading side (C1, J1-1, J1-2)

(b) Fixed side (C1, J1-1, J1-2)

(c) Loading side (C6, J6-1, J6-2)

(d) Fixed side (C6, J6-1, J6-2)

(e) Loading side (C7, J7-1, J7-2)

(f) Fixed side (C7, J7-1, J7-2)

(g) Loading side (C8, J8-1, J8-2)

(h) Fixed side (C8, J8-1, J8-2)

Figure 6: Relationship between the bending moment and deformation angle

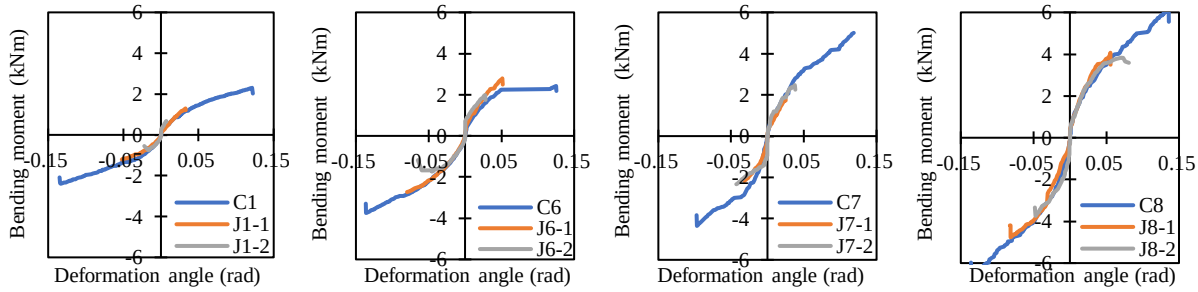

(a) Loading side

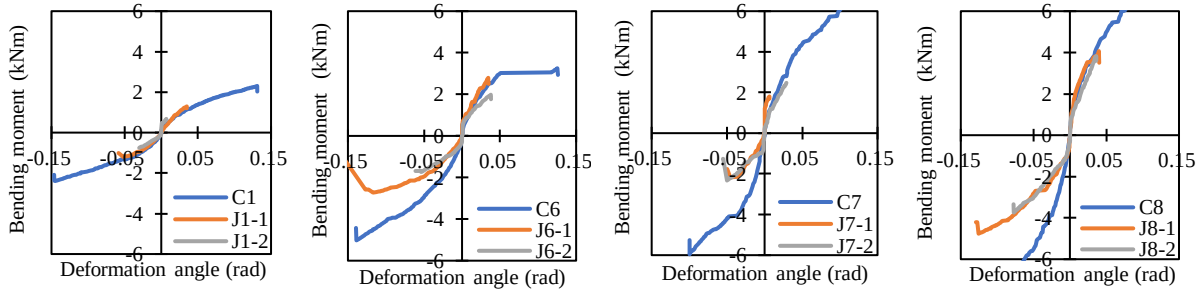

(b) Fixed side

Figure 7: Results of full-scale tests

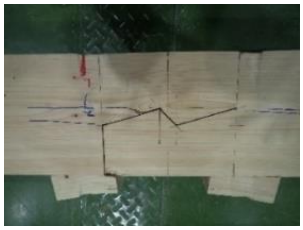

(a) Cleavage failure from *Kama*-joint and bending failure (J8-1)

(b) *Kama*-joint part of the specimen after tests (J8-2)

(c) Shear failure (J1-2)

Figure 8: Failure of oblique scarf joint *nuki*

3 ESTIMATION EQUATION

In this study, theoretical results were calculated using the design equation used for continuous *nuki* in traditional Japanese wooden houses. The rotating stiffness (K_θ) and yield moment (M_y) were evaluated, and the results were compared with those of the full-scale tests.

3.1 Outline of estimate equation for continuous *nuki*

From the design equation of the continuous *nuki* [3], K_θ and M_y are obtained as follows:

$$K_\theta = x_p^2 y_p E_{90} \left\{ \frac{x_p}{Z_0} \left(C_{xm} - \frac{1}{3} \right) + 0.5 \mu C_{xm} \right\} \tag{1}$$

$$M_y = \frac{K_\theta Z_0 F_m}{x_p E_{90} C_{xm} \sqrt{C_{ym}}} \tag{2}$$

$$F_m = \frac{2.4}{3} \times f_{cv} \tag{3}$$

$$C_{xm} = 1 + \frac{4Z_0}{3x_p} \tag{4}$$

$$C_{ym} = 1 + \frac{4Z_0}{3ny_p} \tag{5}$$

$$\theta_y = \frac{M_y}{K_\theta} \tag{6}$$

where x_p is the diameter of half of the column (mm), y_p is the width of the *nuki* (mm), E_{90} is the lateral compressive elastic modulus (N/mm^2), Z_0 is the height of the *nuki* (mm), μ is the coefficient of friction (μ = 0.4 [4]), θ_y is the yield deformation angle (rad), F_m is the embedment yield unit stress (N/mm^2) evaluated from the result of partial compression tests when the edge distance is infinite, f_{cv} is the embedment strength (N/mm^2), C_{xm} and C_{ym} are the embedment growth factors in the *x* and *y* directions, respectively, when the edge distance is infinite, and *n* is the displacement factor between the wood fiber direction and the wood fiber radial direction (n of Japanese cypress is 6, and n of Japanese cedar is 5).

Table 3 provides the material constant which is used for calculation and the ratio of the first and second stiffness from the estimate equation.

The theoretical value of the second stiffness is calculated using the average of the ratio of the first stiffness to the second stiffness from the results of partial compression tests.

Table 3: Material constants

Types of wood	Lateral compressive elastic modulus E_{90} (N/mm^2)	Embedment strength (Partial compressive strength) f_{cv} (N/mm^2)	Embedment yield unit stress f_m (N/mm^2)	Second stiffness / First stiffness (K_2/K_1)
Japanese cypress	239	6.38	5.10	0.094
Japanese cedar	219	4.73	3.78	0.090

3.2 Comparison between theoretical and experimental results obtained for continuous *nuki* specimens

Figure 9 compares the theoretical and experimental values for each continuous *nuki* specimen. The theoretical value was calculated using the average lateral elastic modulus from the results of the material tests. In all continuous *nuki* specimens, the theoretical value of the initial stiffness was greater than the experimental value. This may be caused by the construction tolerances of the specimen and the wood drying shrinkage effect. In addition, the theoretical value, which was calculated using the 50th percentile average of the lateral elastic modulus, was compared with the experimental value to determine the effect of the gap between the column and the *nuki*. As a result, experimental value was between the theoretical values for all

specimens except C5. The gap between the column and the *nuki* in C5 was wider than in the other specimens, because C5 does not have a wedge. Therefore, the experimental results revealed a smaller value than the one that was estimated because the initial stiffness of C5 became smaller than that of the other specimens.

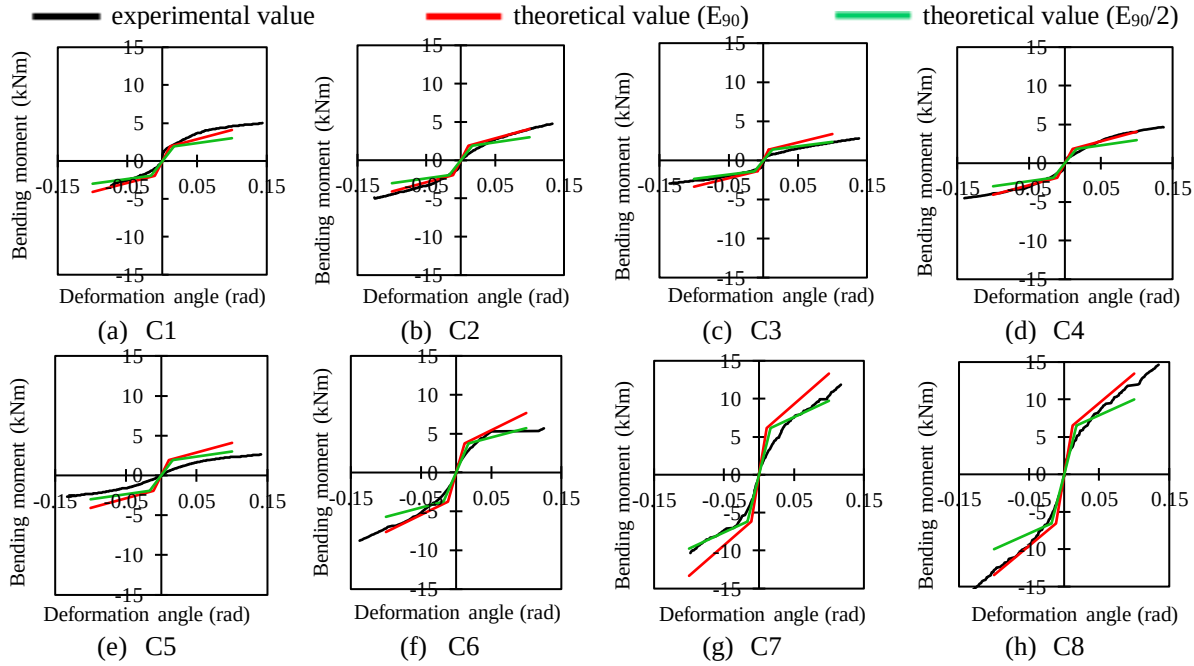

Figure 9: Comparison between theoretical and experimental results obtained for continuous *nuki*

3.3 Estimation equation for oblique scarf joint *nuki*

In the full-scale tests, the specimens with oblique scarf joint *nuki* demonstrated embedment failure, bending failure, shear failure, and cleavage failure. The moment at each failure point was calculated and compared with the corresponding experimental result. Table 4 shows the material constants used for the calculation of the estimation equation.

To calculate the magnitude of the moment that led to the embedment failure, the rotating stiffness K_θ and yield moment M_y were evaluated from the design equation of continuous *nuki*, which was provided by a previous study [3]. This followed the same procedure that was used for the continuous *nuki* (equations (1), (2), (3), (4), (5), and (6)). However, the specimens with oblique scarf joint *nuki* are not symmetrical with respect to the *nuki*. Therefore, the yield moment M_y was divided by two in this case, and the coefficients of friction, μ, were 0.4 and 0.2 on the negative and positive sides, respectively [4].

The moment at the point of bending failure (M_b) was evaluated from the geometrical moment of inertia, I, and bending strength, σ_b, as:

$$M_b = \sigma_b \times \frac{I}{h_e/2} \tag{7}$$

$$I = \frac{y_p \times {h_e}^3}{12} \tag{8}$$

where I is the geometrical moment of inertia (mm^4), σ_b is the bending strength (N/mm^2), and h_e is the distance between an edge of the *nuki* and the shear plane of the oblique scarf joint (mm), as shown in Figure 10.

The moment at the point of shear failure (M_s) was evaluated from the shear strength, τ, as:

$$M_s = \alpha y_p \tau h_e \tag{9}$$

where τ is the shear strength (N/mm^2) and α is the shear distance (mm).

The moment at the point of cleavage failure (M_{uw}) was evaluated using a design equation [5] for cleavage failure if a *nuki* is stressed from the wood fiber and radial direction by equations (10) and (11).

$$M_s = P_{uw} h_e \tag{10}$$

$$P_{uw} = \frac{2}{1} C_r y_p \sqrt{\frac{h_e}{1 - \frac{h_e}{Z_0}}} \tag{11}$$

where P_{uw} is the ultimate strength caused by the cleavage failure and C_r is a cleavage failure constant (N/mm$^{1.5}$) (Japanese cypress $C_r = 10.0$ (N/mm$^{1.5}$)).

Table 4: Material constant

Types of wood	Lateral compressive elastic modulus E_{90} (N/mm^2)	Partial compressive strength F_{cv} (N/mm^2)	Bending strength σ_b (N/mm^2)	Shear strength τ (N/mm^2)
Japanese cypress	250	8.82	72.8	11.7

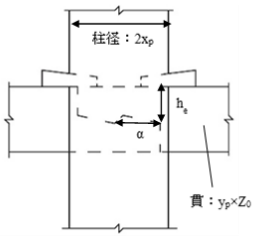

Figure 10: the detail of joint

3.4 Comparison between theoretical and experimental results obtained for oblique scarf joint *nuki* specimens

Figure 11 compares the moments at bending failure, embedment failure, shear failure, and cleavage failure with their associated experimental values for the oblique scarf joint *nuki* specimens. In Figures 11(g) and (h), the moments at the points of bending and shear failure exceeded 10 kNm, and hence these are not shown in the graph.

All specimens with an oblique scarf joint *nuki* first exhibited cleavage failure in the *nuki*, followed by multiple failures. The moment at cleavage failure was the smallest and corresponded to the experimental value. The specimens with an oblique scarf joint *nuki* were already subjected to cleavage failure before the failure was confirmed visually around the *nuki* in the full-scale tests. This was because the cleavage failure occurred in the part of the column–*nuki* joint that is visually inaccessible from the outside. Furthermore, J1-2, J6-2, and J8-2, specimens that exhibited shear failure within the joint after failure, experienced the moment of shear failure.

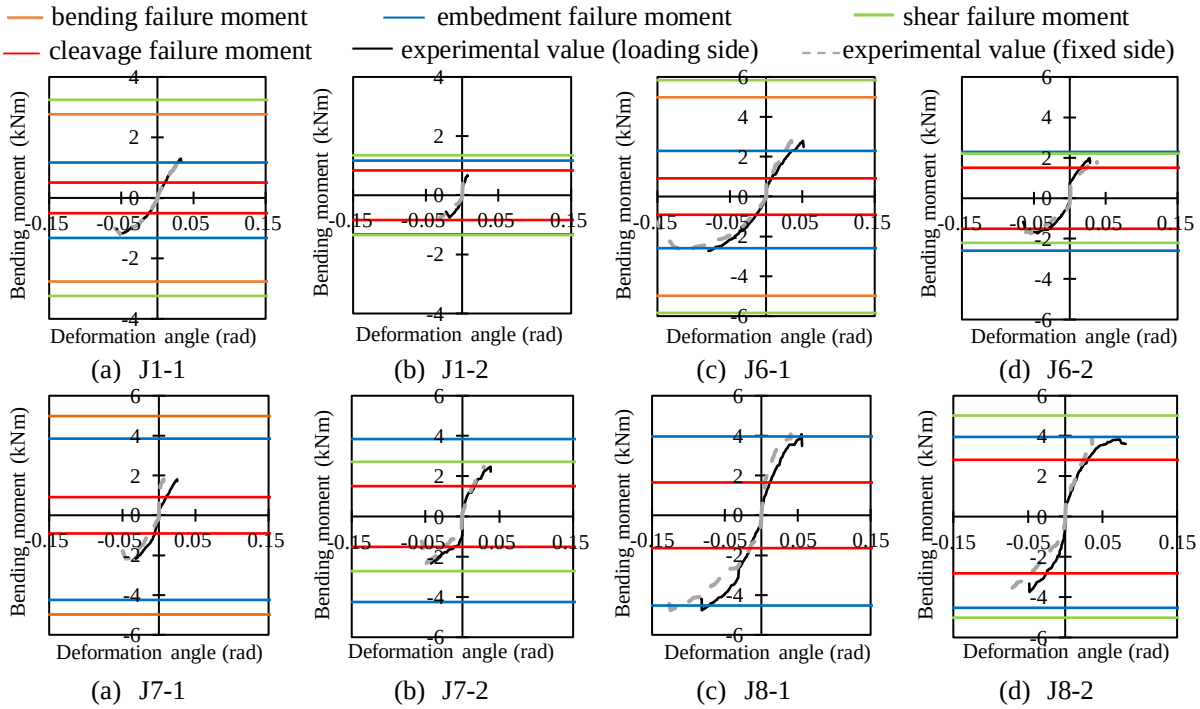

Figure 11: Comparison between theoretical and experimental results obtained for oblique scarf joint *nuki*

4 CONCLUSIONS

We performed full-scale tests to obtain the relationship between the bending moment and deformation angle and failure property of plus-shaped column-*nuki* connections, which of either the continuous or oblique scarf joint *nuki* type. Furthermore, the theoretical values were calculated using the design equation, and the experimental and theoretical values were compared. The main findings of this study are as follows:

- Continuous *nuki* specimens showed cleavage failure at the wedge or column in the full-scale tests; however, this was not affected by the decrease in the bending moment. All oblique scarf joint *nuki* specimens showed cleavage failure first in the *nuki*, followed by multiple failures. The full-scale test results showed that the yield and ultimate bending moment of oblique scarf joint *nuki* specimens were approximately 10 to 70% smaller than those of the corresponding continuous *nuki* specimens.
- In continuous *nuki* specimens, the initial stiffness of the theoretical value was higher

than the experimental one. In addition, the experimental value expected for the C5 specimen without the wedge was within the range of the theoretical values that were calculated using the average lateral elastic modulus and the theoretical values that were calculated using half of the average lateral elastic modulus. The gap between the column and the *nuki* in the specimen without a wedge was bigger than the gap in the other specimens. Therefore, the experimental value of the specimen without the wedge was less than the theoretical one due to the small initial stiffness.

- In the oblique scarf joint *nuki* specimens, the theoretical value of cleavage failure was the smallest, and it coincided with the experimental value. Regarding bending failure and shear failure, the experimental bending moment was smaller than the theoretical value.

The results demonstrated that failure can be partially estimated using the previous design equation by comparing theoretical to experimental values; however, the experimental data on plus-shaped column-*nuki* connections which have oblique scarf joint *nuki* is still insufficient. In the future, more full-scale tests of plus-shaped column-*nuki* connections can be performed, and finite element analysis can be used to create a model which corresponds to various failure properties.

Acknowledgements. This research was supported by the Matsui Kakuhei Memorial Foundation. We gratefully acknowledge this support.

REFERENCES

[1] Kaori Fujita, Isao Sakamoto, Yoshimitsu Ohashi: *A Study on lateral loading test of column and batten (nuki) joint used in traditional wooden architecture (Part 1)*, Summaries of Technical Papers of Annual Meeting, Architectural Institute of Japan, Structures-III, pp. 103-104, 1996.09 (in Japanese)

[2] Editorial Committee for Manual of Seismic Design for Wooden Frame Structures: *Manual of Seismic Design for Wooden Structures Taking Advantage of Traditional Structural Techniques - Methods for Seismic Design and Seismic Reinforcement Design Based on Response-Limit Capacity Analysis* -, Gakugei Shuppan Sha Co. Ltd., Japan, March 2004, pp.79

[3] Architectural Institute of Japan (edited): *Design Manual for Engineered Timber Joints*, Maruzen, Japan, September 2010, pp. 254-257.

[4] Japan Housing and Wood Technology Center: *Project Report about points to consider for design of timber structures* (in Japanese), March 2018, pp. 216-226.

[5] Architectural Institute of Japan (edited): *Standard for Structural Design of Timber Structures*, Maruzen, Japan, March 2009, pp. 36-37.